Gas Adsorption Characteristics of Metal–Organic Frameworks via Quartz Crystal Microbalance Techniques

ARTICLE *in* THE JOURNAL OF PHYSICAL CHEMISTRY C · JULY 2012

Impact Factor: 4.77 · DOI: 10.1021/jp304631m

6 AUTHORS, INCLUDING:

Milad Navaei
Georgia Tech Research Institute
10 PUBLICATIONS **11** CITATIONS
SEE PROFILE

Peter Hesketh
Georgia Institute of Technology
155 PUBLICATIONS **2,336** CITATIONS
SEE PROFILE

THE JOURNAL OF PHYSICAL CHEMISTRY C

Article

pubs.acs.org/JPCC

Gas Adsorption Characteristics of Metal–Organic Frameworks via Quartz Crystal Microbalance Techniques

Anandram Venkatasubramanian,[†] Milad Navaei,[†] Kevin R. Bagnall,[‡] Ken C. McCarley,[‡] Sankar Nair,*[,§] and Peter J. Hesketh*[,†]

[†]G.W. Woodruff School of Mechanical Engineering, Georgia Institute of Technology, Atlanta, Georgia 30332, United States

[‡]Gas Separation Technology Research & Development, ConocoPhillips Company, Bartlesville, Oklahoma 74004, United States

[§]School of Chemical & Biomolecular Engineering, Georgia Institute of Technology, Atlanta, Georgia 30332, United States

Supporting Information

ABSTRACT: We report an experimental investigation of the adsorption properties of two important small-pore metal–organic framework (MOF) materials recently identified for gas separation applications, through the development and use of a high-pressure/high-temperature quartz crystal microbalance (QCM) device. In particular, we characterize in detail the CO_2, CH_4, and N_2 adsorption characteristics of the MOFs Cu(4,4′-(hexafluoroisopropylidene)bisbenzoate)$_{1.5}$ (referred to as Cu–hfipbb) and zeolitic imidazolate framework-90 (ZIF-90). We first describe the construction of a QCM-based adsorption measurement apparatus. Single-component adsorption isotherms of CO_2, CH_4, and N_2 in the two MOFs were then measured at temperatures ranging from 30 to 70 °C and pressures ranging from 0.3 to 110 psi. In both materials, the order of adsorption strength is CO_2 > CH_4 > N_2. We find that adsorption in the 1-D channels of Cu–hfipbb can be well described by a single-site Langmuir model. On the other hand, adsorption in ZIF-90 follows a more complex behavior, commensurate with its pore structure consisting of large porous cages connected in three dimensions by small windows. The nongravimetric QCM-based measurement techniques are shown to be a valuable microanalytical tool for the study of molecular adsorption in MOFs.

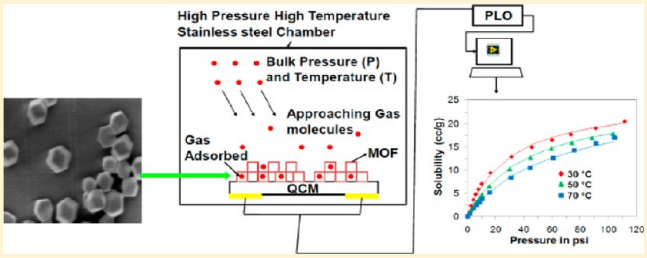

1. INTRODUCTION

Nanoporous molecular sieve materials have found a wide range of technological applications in catalysis, separations, and ion exchange.[1] Metal–organic frameworks (MOFs) are a relatively new class of crystalline nanoporous materials with features such as tailorable pore structure, tunable pore sizes for molecular sieving, high surface area, and the possibility of introducing analyte-specific adsorption sites. MOFs are synthesized by coupling inorganic clusters with organic "linker" groups,[2] yielding rigid but open frameworks that can accommodate guest molecules. Several reports of their use in the fabrication of membranes for gas separations have appeared.[3−6] Their use in adsorption-based applications is also of considerable interest, and they have been shown to selectively adsorb specific gas molecules from mixtures.[7−15]

Because of the importance of MOFs as membrane materials and adsorbents, and considering the large number of MOF materials available, there is a need to develop efficient strategies for screening and measuring the adsorption characteristics of key MOF materials for a given potential application. We have recently proposed such a strategy to enable the use of MOFs in gas separation membrane and adsorption applications. The first step of this strategy involves the use of computational approaches to screen large numbers of MOF materials and predict their effectiveness for a particular separation via a hierarchical series of molecular simulations.[16,17] Through this method, large numbers of MOFs can be eliminated as being unsuitable for a particular application, and a reasonable number of potentially suitable MOF materials are predicted, which then become the target of more focused and efficient experimentation to determine the adsorption and diffusion characteristics. The characterization of gas adsorption in porous materials is often performed by gravimetric or volumetric equipment. Their capital and operating costs are generally high. Furthermore, they require relatively large amounts of sample (typically >100 mg) to obtain accurate data and also cannot measure gas adsorption in thin films or coatings. It is therefore desirable to broaden the range of techniques that can be used to measure the adsorption properties of MOF materials over a substantial range of pressure and temperature by nongravimetric methods, ideally with only a small sample size requirement (<1 mg) and with the sample being potentially in powder, coating, or thin film form.[18−20]

In this paper, we investigate the characterization of the adsorption properties of two recently identified MOF materials through the development and use of a high-pressure/high-

Received: November 7, 2011
Revised: June 24, 2012
Published: June 26, 2012

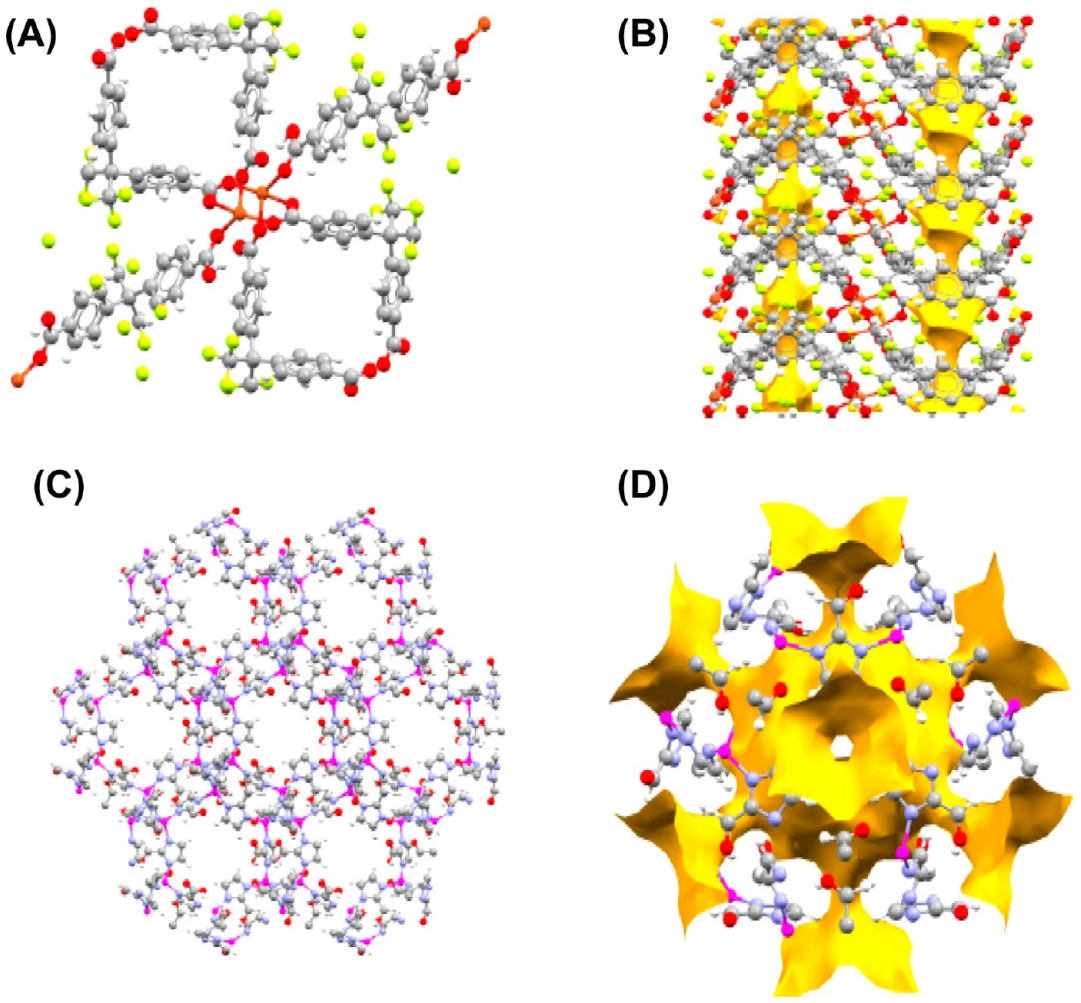

Figure 1. (A) Structure of Cu(hfipbb)(H_2hfipbb)$_{0.5}$ in the [010] direction and (B) in the [100] direction. The latter structure schematically shows the one-dimensional channels available for molecular adsorption and diffusion with the void filled topology. (C) Topology of the ZIF-90 structure in the [111] direction and (D) its comparison to the single unit void filled topology.

temperature quartz crystal microbalance (QCM) device. The QCM measures changes in the mass of material deposited on a piezoelectric quartz substrate by measuring the change in its resonant frequency resulting from a change in total deposited mass. QCM devices have been shown to be effective in vacuum, gas phase, and (more recently) in liquid environments.[21,22] Unlike gravimetric measurements, the resonant frequency measurements can be easily made to a high precision, thereby allowing operation with very small amounts of sample. No buoyancy corrections are required. In addition to the resonant frequency, the method also yields data on the dissipation (damping) in the system and thereby allows quantification of the sample's elastic properties that may be useful in thin film/membrane applications. A QCM system can be constructed for a fraction (~20%) of the cost of a gravimetric apparatus. Recent reports have investigated the use of flow cell based QCM techniques for measuring the adsorption and diffusion of volatile organic compounds (VOCs) in MOF materials.[23,24] However, the capability to perform accurate QCM-based adsorption measurements over a comprehensive range of temperature and pressure remains a desirable goal.

In this report, we characterize in detail the CO_2, CH_4, and N_2 adsorption characteristics of two important MOF materials, identified for gas separation applications by computational screening. The two MOF materials of interest are Cu(4,4′-(hexafluoroisopropylidene)bisbenzoate)$_{1.5}$ (referred to as Cu–hfipbb) and zeolitic imidazolate framework-90 (ZIF-90). These materials have been the subject of several recent works that investigate their CO_2, CH_4, and N_2 gas adsorption/transport properties computationally and through the fabrication of membranes.[3,16,17,25] Cu–hfipbb (Figure 1A,B) is a crystalline interpenetrating framework containing 1D channels and is based on a Cu_2(hfipbb)$_4$(H_2hfipbb)$_2$ paddle-wheel building unit. This MOF has cages of effective pore dimensions 5.1 Å × 5.1 Å connected by small windows of dimensions 3.5 Å × 3.2 Å.[17] Previous reports have experimentally characterized the adsorption properties of alkanes (propane, butane, and pentane),[26] argon,[27] and hydrogen[28] in Cu–hfipbb. Recently, Bao et al.[29] characterized the CO_2 and CH_4 gas adsorption process in Cu–hfipbb up to 1 atm pressure. Comparison of experimental isotherm for the corresponding range yielded good agreement. The topology of the ZIF-90 structure is identical to the sodalite silicate topology (Figure 1C,D). The crystal structure comprises of Zn(II) centers linked by imidazolate-2-carboxyaldehyde (ICA) molecules. This leads to a ZIF structure containing cages of size 11.2 Å connected by windows of size 3.5 Å (Figure 1C). Although previous authors have fabricated and tested membranes containing ZIF-90,[30]

very little is known about the intrinsic adsorption and transport properties of this material.

In this work, we first describe the construction and setup of the nongravimetric QCM-based adsorption measurement apparatus. We then present an example of QCM-based gas adsorption measurements by measuring the CO_2 adsorption properties of a polyimide (Matrimid) film and extracting the adsorption thermodynamic parameters, which are then compared to the established properties of this material. Subsequently, we present detailed adsorption measurements for the two MOF materials of interest and discuss the results in terms of simple analytical adsorption models.

2. METHODS

2.1. MOF Crystal Synthesis. Cu−hfipbb crystals were synthesized by the procedure of Carson et al.[31] To synthesize Cu−hfipbb, 4,4′-(hexafluoroisopropylidene)bis(benzoic acid) (98%), copper(II) nitrate hemi(pentahydrate) (98%), and 2-propanol (99.5%) were used as purchased from Sigma-Aldrich. A 200 mg quantity of H_2hfipbb was dispersed in 75 mL of deionized water by shaking and sonication. In a separate container, 79 mg of copper(II) nitrate hemi(pentahydrate) was dissolved in 5 mL of water and 1 mL of isopropanol. The molar ratio of copper nitrate to H_2hfipbb to water was 1:1.5:12900. The two solutions were then mixed and placed in an ice bath and sonicated for 6.6 h with a Sonics Vibracell VCX 130 sonication horn at 77 W, whereupon crystals of Cu−hfipbb precipitated from the solution and were recovered by centrifugation and washing with water.

The synthesis procedure for ZIF 90 crystals was obtained from Bae et al.[3] To synthesize ZIF-90, 20 mmol (1.920 g) of imidazole carboxyaldehyde (ImCA) was added to 50 mL of DMF and heated to 70 °C for 1 h until dissolved. After cooling to room temperature, 5 mmol (1.485 g) of zinc nitrate hexahydrate dissolved in 50 mL of methanol was poured into the DMF/ImCA mixture and stirred for 30 min. The crystals were purified by three cycles of centrifugation and washing with MeOH. The identity and high crystallinity of the synthesized MOF materials were verified by X-ray diffraction.

2.2. Deposition of MOF Crystals and Matrimid Film on QCM Substrates. A 3 g/L suspension of MOF crystals was formed in a solvent (Cu−hfipbb/isopropanol or ZIF-90/methanol) and sonicated for 60 min. Cu−hfipbb crystals were deposited on the QCM substrate by spin-coating from the suspension at 150 rpm. A 50 μL volume of the suspension was added at a time and allowed to evaporate. After an interval of 0.5−1 min, another 50 μL aliquot was added. A total of 500 μL volume was used in this manner. On the other hand, ZIF-90 crystals were drop-coated by depositing about 100 μL on the QCM substrate. The substrates were then prebaked in an oven at 195 °C and atmospheric pressure for 30 min. The samples were then mounted in the measurement apparatus and degassed *in situ* at a temperature of 185 °C under vacuum for about 12 h before adsorption measurements. To prepare the polymer sample, a 0.3 g suspension of Matrimid (Hutzman) was dissolved in 3 g of *N*-methylpyrrolidone (99.5%, anhydrous, VWR Scientific) and spin-coated on the QCM substrate at 2000 rpm. The sample was then prebaked in a conventional oven at 120 °C and atmospheric pressure for 30 min. The sample was then mounted in the measurement apparatus and degassed *in situ* at a temperature of 120 °C under vacuum before adsorption measurements for about 12 h.

2.3. QCM Measurement Cell Design. Figure 2 shows a schematic of the QCM measurement setup, and a labeled

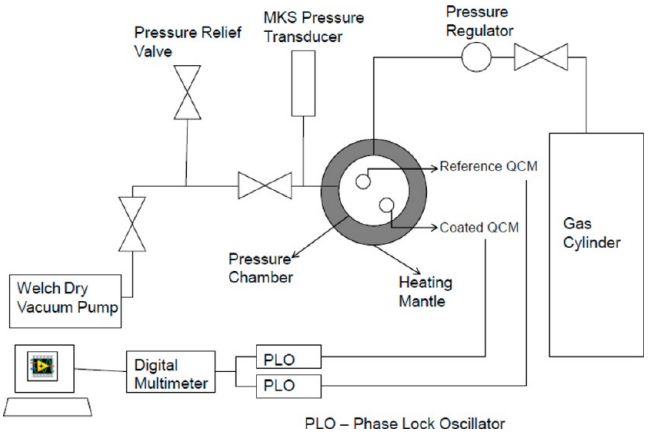

Figure 2. Schematic of the QCM-based adsorption measurement apparatus.

photograph is shown in the Supporting Information. The QCMs employed in this study were purchased from Inficon, NY. They had a resonant frequency of 5 MHz, were cut at room temperature, and had polished gold electrodes on both sides. Two identical crystals were placed inside a 175 mL high-pressure stainless steel cylindrical chamber with a custom-designed QCM holder. One crystal was uncoated and acts as a reference sample, while the other was coated with the material to be studied. The sample environment chamber was constructed from stainless steel SS 316 and can be operated in a range of up to 10 bar pressure and up to 320 °C temperature. The pressure limit is determined by the range of the pressure sensor, whereas the temperature limit is due to the maximum operating temperature recommended for the O-ring (Markez Z1213 perfluoroelastomer, size 236) used to seal the chamber at high pressure. The chamber was placed in a temperature control mantle and connected to an oil-free, dry vacuum pump (Gardner-Welch, CO). The O-rings and the chamber were cleaned periodically with a dry clean cloth and were blown with a jet of dry air to prevent any contaminants from settling in the chamber.

The two crystals were connected through four Bayonet−Neill−Concelman (BNC) connections via high-temperature-resistant cables to two phase-lock oscillators (PLO-10, Inficon, NY). The output frequencies and damping voltages of both QCMs were measured by a frequency counter (Agilent 5313X Series) and an Acquisition/Switch unit (HP 34970A) from the PLO-10. Two K-type thermocouples were used to monitor the temperature at two different locations inside the chamber to ensure that any temperature gradients are negligible. In order to monitor the absolute pressure inside the cell, a pressure transducer (MKS, 10 000 Torr) was connected in the sample chamber, and the pressure was recorded by a pressure reader (PDR200). The pressure was controlled by dosing small amounts of gas into the cell to reach each new equilibrium condition. The temperatures, frequency changes due to the mass adsorbed, and damping voltages were recorded with the LabView software. The sample chamber was placed inside two hemispherical heating mantles and further insulated using glass wool. A digital temperature controller (CG-15001) was used to control the temperature with a precision of ±1 °C. The gases used were research-grade and contained less than 1 ppm of

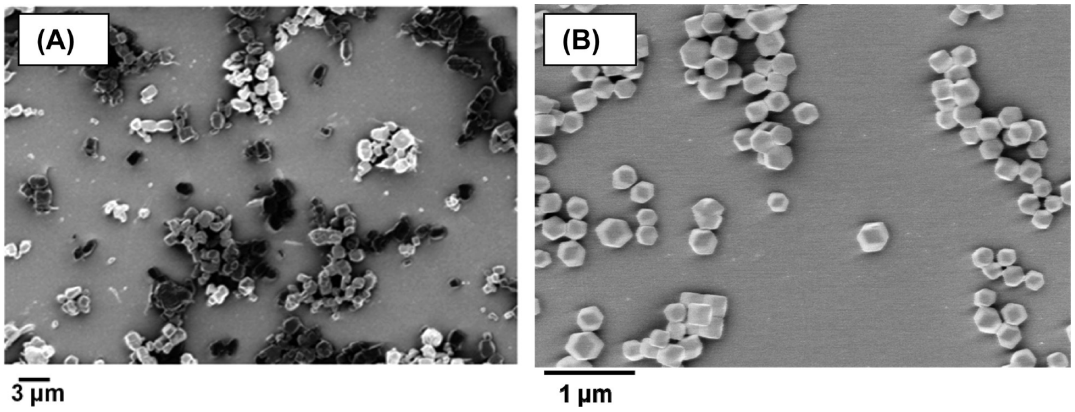

Figure 3. (A) Cu−hfipbb crystals deposited on the gold surface of the QCM. (B) ZIF 90 crystals deposited on the gold surface of the QCM.

water vapor. The current apparatus is only equipped with a heating mantle but does not reach subambient temperatures. It is, in principle, possible to conduct subambient measurements with an appropriate cooling arrangement.

2.4. Measurement Theory. The QCM is a thickness shear mode resonator in which acoustic waves propagate normal to the crystal surface.[32] The use of QCMs as chemical sensors has its origins in the work of Sauerbrey and King. The shift in the resonant frequency of an oscillating AT-cut crystal is correlated quantitatively with addition or removal of mass from the surface of the device. AT-cut crystals are singularly rotated *Y*-axis cuts having thickness shear vibration mode (top and bottom half of the crystal move in opposite direction) during oscillation. The advantages of QCMs over conventional gravimetric devices are compactness, absence of buoyancy effects, and much higher sensitivity per unit sample mass.[32] Mass changes are obtained from the Sauerbrey equation

$$\Delta m = \frac{(f_q - f)\sqrt{\rho_q \times \mu_q}}{2n \times f^2} \quad (1)$$

wherein Δm is the change in mass per unit area as a function of shift in resonant frequency (g/cm^2), f_q is the resonant frequency (Hz) of the reference state, f is the resonant frequency of loaded crystal, ρ_q is the density of quartz (2.648 g cm^{-3}), μ_q is the effective piezoelectrically stiffened shear modulus of quartz (2.947×10^{11} g cm^{-1} s^{-2}), and n is the resonant frequency mode (in this case, $n = 1$). It is assumed that the material deposited has the same acoustic−elastic properties as the substrate. This assumption holds for thin films and small amounts of powder/particulate samples and is validated by comparing the resonant frequency of the unloaded crystal with the resonant frequency of the sample-loaded crystal. A common rule of thumb is that the shift in resonant frequency due to mass addition should be less than 1% for the Sauerbrey equation to be valid.[33] This was strictly true in all of our measurements. The resonant frequency of the QCM is affected by the following factors:

$$f = f_0 + \Delta f_m + \Delta f_T + \Delta f_P + \Delta f_v + \Delta f_R \quad (2)$$

Here f_0 is the fundamental resonant frequency, Δf_m is the shift in frequency due to mass change, Δf_T is the shift in frequency due to temperature changes, Δf_P is the shift in frequency due to pressure changes, Δf_v is the shift in frequency due to viscosity, and Δf_R is the shift in frequency due to "roughness loading" (i.e., shear caused by the ambient medium). All our experiments were conducted under isothermal conditions, and the bulk medium is a low-viscosity gas. Hence, the temperature, viscosity, and roughness loading factors are negligible. Previous research has shown that gas adsorption in sorbent powders deposited on the QCM is negligibly affected by elasticity effects and can be described with Sauerbrey's equation.[34] An accurate pressure correction is performed by subtracting the response of the reference QCM from that of the sample-coated QCM. It is well-known that the precision of the 1 in. diameter QCM is about 0.1 μg (100 ng),[35] which translates to ~5 ng/cm^2. In our apparatus, we have measured the resonant frequency up to 12 decimal places with a digital multimeter. We found that the QCM resonant frequency shift is measured with a precision of ~0.5 Hz, which translates to about 0.18 μg (9 ng/cm^2).

2.5. Adsorption Measurements and Analysis. We first validated the accuracy of the QCM apparatus using a well-known polymer as a standard material. In particular, we measured adsorption isotherms for CO_2 in the poly(imide) Matrimid 5218 up to 60 psi of pressure and at temperatures between 25 and 52 °C. Adsorption in Matrimid was analyzed using the well-known dual mode adsorption isotherm for glassy polymers.[36−38] The Henry's law coefficient within this expression was correlated with the Lennard-Jones potential well depth parameter (ε/κ) for the penetrating gas.[38]

$$C = K_D P + \frac{C_H \times \alpha P}{1 + \alpha P} \quad (3)$$

$$K_D = K_{D0} e^{m\varepsilon/\kappa T} \quad (4)$$

$$C_H = C_{H0} e^{-\Delta H_a/RT} \quad (5)$$

where C is the adsorbed gas concentration at STP (cm^3/cm^3), K_D is the temperature-dependent Henry's coefficient (cm^3/cm^3·psi), K_{D0} is the temperature-independent part of the Henry's coefficient (cm^3/cm^3·psi), and m is a constant parameter independent of penetrant or the nature of the adsorbent. From Scholes et al.,[38] $m = 6.67 \pm 0.5$. The Lennard-Jones potential well depth parameter (ε/κ) is obtained from Poling et al.[39] as 195.2 K. In the Langmuir part of the expression, C_H is the temperature-dependent Langmuir adsorption capacity (cm^3/cm^3), C_{H0} is the temperature-independent part (cm^3/cm^3), ΔH_a is the heat of adsorption (kJ/mol), α is the temperature-independent Langmuir adsorption constant (psi^{-1}), and P is pressure (in psi). In order to fit the adsorption data from glassy polymers, this

model includes a temperature-dependent Henry's coefficient and Langmuir adsorption capacity, whereas the Langmuir parameter α is assumed to be temperature-independent.

Single-component adsorption isotherms of CO_2, CH_4, and N_2 in the two MOFs were then collected at different temperatures ranging from 30 to 70 °C and pressures ranging from 0.3 to 110 psi (about 7.5 atm). Measurements were taken in pressure intervals of 2−3 psi (below 1 atm) and ∼14 psi (above 1 atm). The experimental isotherms were then analyzed in terms of a simple Langmuir model to obtain thermodynamic parameters like adsorption capacity and heat of adsorption:

$$C = \frac{C_H \times \alpha P}{1 + \alpha P} \quad (6)$$

$$\alpha = \alpha_0 \times e^{(-\Delta H_a/RT)} \quad (7)$$

where C_H is now a temperature-indepdent Langmuir adsorption capacity (cm^3/g), α is now the temperature-dependent Langmuir constant (psi^{-1}), and α_0 is the temperature-independent part (psi^{-1}).

3. RESULTS AND DISCUSSION

3.1. Material Characterization. Following the MOF material deposition on the QCM, the samples was examined by scanning electron microscopy (SEM) and by powder X-ray diffraction (PXRD) before and after the adsorption measurements to ensure that the structure of the MOF was preserved throughout the experiment. From the SEM images in Figure 3A, it is apparent that the Cu−hfipbb crystals have a size distribution ranging from 0.5 to 2 μm and the distribution of the sample on the QCM is not uniform as we can see patches of the gold substrate. The size distribution of the ZIF-90 particles was considerably narrower (300−500 nm, Figure 3B). The PXRD patterns of the deposited MOF samples, obtained before and after the adsorption measurement, were generally consistent with the simulated PXRD patterns of highly crystalline Cu−hfipbb (see Figure 4A) and ZIF-90, respectively (see Figure 4B). However in Figure 4A, there is a slight shift in peak intensity between experiments. Many MOFs show minor structural changes (as seen by XRD) after activation and sorption measurements. The sources of these changes are yet poorly understood. Two possible reasons are the loss of residual solvent molecules during activation or slight disorder induced by heating.

3.2. CO_2 Adsorption in Matrimid. Following the initial preheating at 120 °C under vacuum, the chamber was cooled down to room temperature and the mass of Matrimid deposited was found by measuring the shift in resonant frequency. The deposited mass was measured to be 364 μg. Then, single-component CO_2 adsorption isotherms were collected at temperatures of 25, 42, and 52 °C and pressures up to 60 psi. Figure 5 shows the experimental and fitted dual-mode adsorption isotherms for CO_2 in Matrimid (eqs 3−5). The adsorption parameters obtained from our QCM-based measurement are compared against the adsorption parameters obtained gravimetrically by Scholes et al.[38] in Table 1. In Table 1, we observe a very good agreement between the thermodynamic parameters obtained from our experimental results and those obtained by Scholes et al.[38] There are some minor quantitative differences, which are possibly due to differences in polymer film casting techniques, effects of physical aging of the polymer, and differences in penetrant gas purity.[38] The presence of such effects is not entirely avoidable. The average relative % error (ARE) between the model and the experimental data is shown in Table S1 (Supporting Information), corroborating the generally high quality of the fit results. Hence, it is clear that our QCM-based apparatus gives reliable results and can be used reliably for microanalytical adsorption measurements.

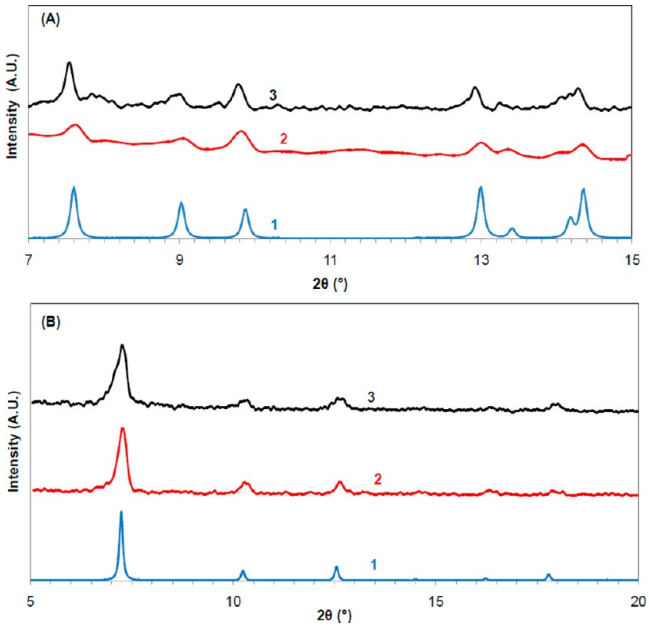

Figure 4. XRD patterns of (A) Cu−hfipbb crystals and (B) ZIF-90 crystals, taken before (marked as **2**) and after (marked as **3**) adsorption measurements, and comparison with the simulated XRD patterns of the crystal structures (marked as **1**).

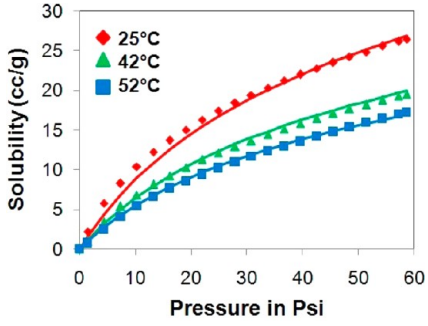

Figure 5. Solubility of CO_2 at STP per unit volume of Matrimid 5218 at different temperatures as measured by the QCM technique and comparisons to literature measurements using gravimetric techniques.

Table 1. CO_2 Adsorption Parameters for Matrimid 5218 Obtained from the QCM-Based Measurement and Comparison to Parameters Obtained from Gravimetric Measurements[38]

parameter	QCM	gravimetric
C_{H0} (cm^3/cm^3)	0.09 ± 0.006	0.08 ± 0.031
ΔH_a (kJ/mol)	−14.6 ± 0.93	−14.9 ± 0.97
α (psi^{-1})	0.031 ± 0.002	0.034 ± 0.0023
K_{D0} ($cm^3/cm^3 \cdot psi$) × 10^{-3}	1.36 ± 0.09	1.23 ± 0.682
m	6.53 ± 0.4	6.67 ± 0.5

3.3. Gas Adsorption in Cu−hfipbb. Following the initial degassing at 185 °C under vacuum, the chamber was cooled down to room temperature and the mass of Cu−hfipbb MOF

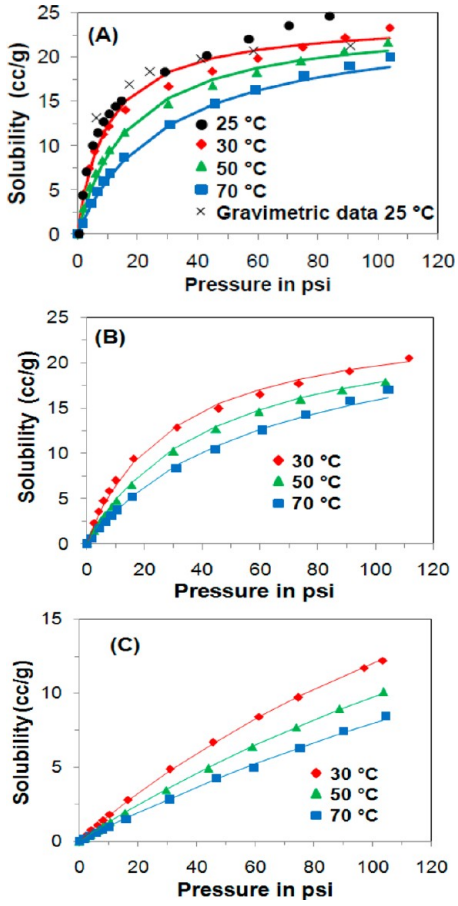

Figure 6. Solubility of gases (in cm^3 STP/g) at 25 (only CO_2), 30, 50, and 70 °C in the MOF Cu−hfipbb. (A) CO_2 adsorption isotherms at different temperatures, with a gravimetrically measured CO_2 adsorption isotherm at 25 °C. (B) CH_4 and (C) N_2 adsorption isotherms at different temperatures. Langmuir model fits are represented by the solid lines.

deposited was measured to be 404.7 μg (sample 1). Gas adsorption isotherms were then collected at temperatures 30, 50, and 70 °C for pressures up to 100 psi. Figures 6A−C show the adsorption isotherms for CO_2, CH_4, and N_2 on Cu−hfipbb at different temperatures. An additional CO_2 gas adsorption isotherm was obtained at 25 °C and compared to available gravimetric data 25 °C (Figure 6A). The mass of Cu−hfipbb MOF deposited on the QCM for this comparison was 262.4 μg (sample 2), and the sample preparation and pretreatment procedure was the same as in sample 1. At low and moderate pressures, there is good agreement of the two isotherms, but at higher pressures there is some deviation. The reasons for this behavior are not fully understood; however, the QCM isotherms were fully reproducible between samples 1 and 2. The adsorption isotherms (at 30−70 °C) obtained from the QCM-based high-pressure sorption apparatus were then fit with the Langmuir isotherm (eqs 6 and 7), and the key adsorption properties (enthalpy of adsorption, adsorption capacity, and pre-exponential entropic factor) were obtained as shown in Table 2. The average relative % error (ARE) between the model and the experimental data is shown in Table S2 (Supporting Information).

A fundamental assumption of the Langmuir model is that adsorption occurs as a monolayer on the internal pore surfaces of the material, with all surface binding sites being equivalent

Table 2. Adsorption Parameters for Cu−hfipbb Based on the Langmuir Model

gas	C_H (cm^3/g)	α_0 (psi^{-1}) × 10^{-6}	ΔH_a (kJ/mol)
CO_2	24.1 ± 0.61	20.3 ± 0.52	−21.3 ± 0.54
CH_4	25.4 ± 0.52	56.3 ± 1.15	−16.1 ± 0.33
N_2	37.8 ± 0.99	33.4 ± 0.88	−12.4 ± 0.33

and accommodating one adsorbed molecule. Furthermore, the ability of a molecule to adsorb at a given site is independent of the occupancy of neighboring sites. As explained earlier, Cu−hfipbb is a crystalline interpenetrating MOF containing 1D channels and has cages of dimensions 5.1 × 5.1 Å connected by smaller windows of dimensions 3.5 Å × 3.2 Å as shown in Figure 1A,B. The kinetic diameters of CO_2, CH_4, and N_2 molecules are 3.3, 3.8, and 3.6 Å, respectively.[40] Considering the comparable dimensions of the pore channels and the kinetic diameters of the gas molecules, we can infer that the penetrant gases are most likely to adsorb in a monolayer, hence leading to a good fit of the Langmuir model to obtain the adsorption properties. Further previous research has shown that materials like Cu−hfipbb which have comparable structures to zeolites and other porous materials[29,41,42] can be modeled with Langmuir isotherm model. From our experimental results we see that the adsorption capacity of CO_2, CH_4, and N_2, as well as the heat of adsorption, are in decreasing order. It is clear that CO_2 shows the strongest adsorption affinity toward the Cu−hfipbb framework, owing to its quadrupole moment.[17] Although the kinetic diameter of CH_4 is slightly greater than that of N_2, which may cause it to diffuse more slowly in the material, it is thermodynamically more favored for adsorption in Cu−hfipbb than N_2.

Comparing the current experimental results with the previous simulation study,[17] it is seen that the experimental single-component adsorption isotherms of CO_2 (at 25 and 30 °C) in Cu−hfipbb compares well with the simulated single-component adsorption isotherm at 25 °C at high pressures (>1 atm), while at low pressures the predicted adsorption is higher than the experimental measurements. This strongly indicates that the force field models and atomic charges used to simulate the adsorbate−framework interactions may require fine-tuning. At higher pressures, adsorbate−adsorbate interactions dominate, and better agreement of the simulations with experimental data is seen. Single-component methane adsorption simulations in Cu−hfipbb at 25 °C were also reported recently.[17] A trend similar to that of CO_2 is seen in the comparison of experimental and simulated data. We also compared the heats of adsorption of CO_2 and CH_4 from the simulation results (−9.7 kJ/mol for CO_2 and −5.8 kJ/mol for CH_4) with the experimentally obtained heats of adsorption (−21.3 kJ/mol for CO_2 and −16.1 kJ/mol for CH_4). The experimental results suggest that quantitative interpretation of currently available adsorption simulation data in Cu−hfipbb must be made with caution. As mentioned earlier,[17] errors in estimation of interatomic forces (e.g., the attractive dispersion forces) could have a significant impact on the accuracy of computational predictions.

3.4. Gas Adsorption in ZIF-90. Following the vacuum degassing at 185 °C, the sample chamber was cooled to room temperature, and the mass of the ZIF-90 MOF deposited on the QCM was measured. For gas adsorption measurements using ZIF-90, two samples were prepared. Sample 1 was measured to have 164 μg of ZIF-90 and was suitable for CO_2 and CH_4 adsorption measurements. N_2 adsorption isotherms

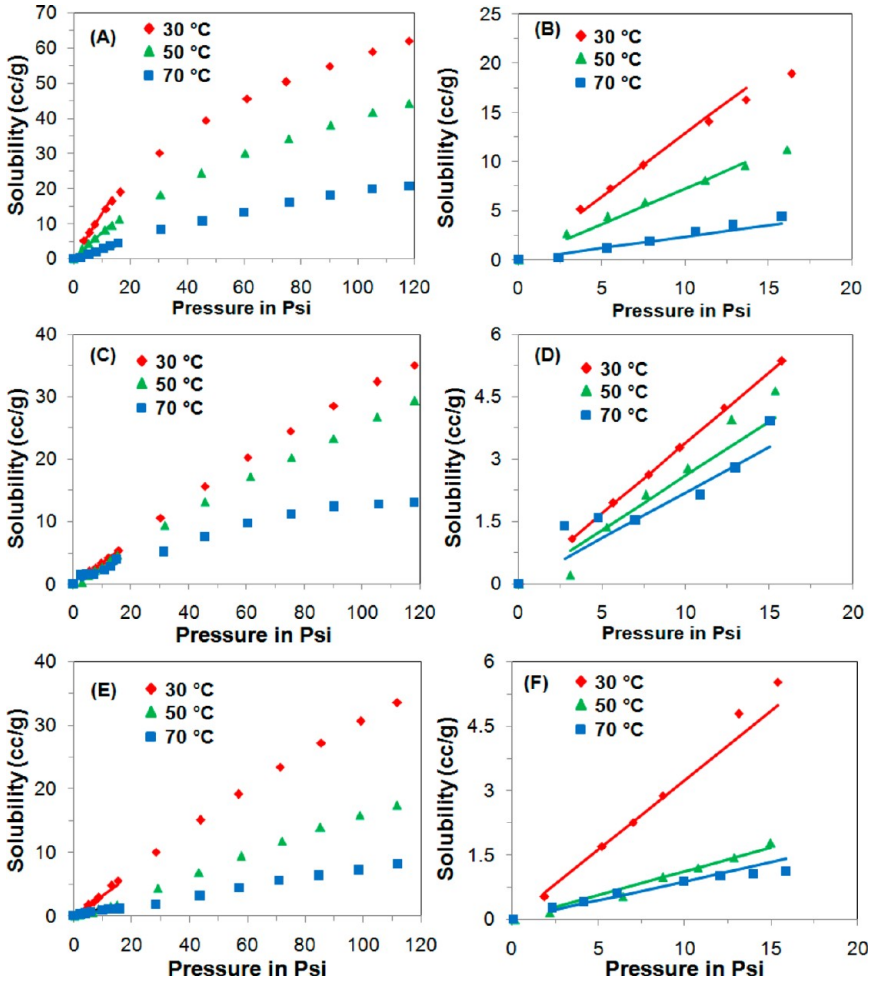

Figure 7. Solubility of gases (in cm^3 STP/g) at 30, 50, and 70 °C in the MOF ZIF-90. CO_2 (A, B), CH_4 (C, D), and N_2 (E, F) adsorption isotherms for the entire pressure range studied and the subatmospheric pressure range. Henry's constant is fitted in the subatmospheric pressure range as represented by the solid lines.

were measured with sample 2 (258 μg of ZIF-90), since N_2 was found to adsorb quite weakly in ZIF-90 and a larger sample is required in order to obtain valid results. Separate samples were used for CO_2, CH_4, and N_2, and furthermore adsorption isotherms from different samples were measured for CO_2 and CH_4 at 30 °C for the same pressure range and were found to be identical. The adsorption isotherms for ZIF-90 were collected at temperatures of 30, 50, and 70 °C and pressures up to 110 psi. Figures 7A–F show the gas adsorption isotherms for CO_2, CH_4, and N_2 collected at different temperatures. These adsorption isotherms were first fit with the Langmuir model. However, a poor fit of the experimental data was obtained. The ZIF-90 pore structure comprises large cages of size 11.2 Å connected by small windows of size 3.5 Å. Considering the pore structure and the kinetic diameter of the gas molecules considered in this paper, it is clear that adsorption will not obey a Langmuir model at moderate and higher pressures, due to possible multilayer adsorption in the cages. Therefore, one can only obtain parametric information on the adsorption characteristics in the low-pressure regime wherein Henry's law can be applied (Table 3, Figures 7D–F). The average relative % error (ARE) between the model and the experimental data is shown in Table S3. It is found that CO_2 is the most thermodynamically favored, followed by CH_4 and then N_2. As expected, the Henry's constants decrease with increasing temperature. The detailed gas adsorption data presented in this work facilitates further detailed analyses using statistical thermodynamic models and molecular simulations of gas adsorption in ZIF-90, which serves as a good exemplar of the ZIF class of porous materials.

Table 3. Henry's Constants for Gas Adsorption in ZIF-90

K_H (cm^3/g·psi)	30 °C	50 °C	70 °C
CO_2	1.28 ± 0.05	0.73 ± 0.05	0.23 ± 0.02
CH_4	0.34 ± 0.003	0.26 ± 0.023	0.22 ± 0.015
N_2	0.32 ± 0.022	0.11 ± 0.02	0.088 ± 0.01

4. CONCLUSION

Metal–organic frameworks are a rapidly developing class of materials with immense potential in the areas of molecular separation, catalysis, and sensing, among many others. Experimental knowledge of the adsorption characteristics of MOFs are a critical component of progress in the science and engineering of these materials. In this paper, we have reported the development and application of a controlled-pressure and controlled-temperature QCM-based system for adsorption measurements in nanoporous materials and demonstrated its use by studying gas adsorption in two important small-pore MOF materials widely considered for separation applications.

The apparatus was first validated by gas adsorption measurements of a polyimide material. Detailed CO_2, CH_4, and N_2 adsorption studies were then carried out on the two MOF materials (Cu−hfipbb and ZIF-90). The adsorption isotherms were then fit to simple analytical models and key adsorption thermodynamic parameters were obtained. Cu−hfipbb was found to obey Langmuir adsorption behavior, consistent with its pore structure composed essentially of 1D channels without significant cage-like spaces. On the other hand, the cage−window duality present in ZIF-90 leads to large deviations from Langmuir adsorption. In both MOF materials, the order of adsorption affinity was $CO_2 > CH_4 > N_2$, reflecting the stronger polar interactions of the MOF frameworks with CO_2 molecules. In summary, the QCM-based adsorption measurement technique is shown to be valuable in the quantitative and qualitative study of molecular recognition by nanoporous MOF materials. Although more compact/miniaturized microanalytical techniques such as QCM show promise for future adsorption and diffusion measurement methodologies, further developments will require the development of appropriate protocols for reliable and routine sample preparation of the loaded QCM crystals. The results from the present, and forthcoming, studies are also expected to be useful in validating and parametrizing analytical and molecular (force-field) models for adsorption in MOF materials.

■ ASSOCIATED CONTENT

Supporting Information

A labeled photograph of the QCM-based adsorption measurement setup and tables quantifying error bars in the fitting of the adsorption data. This material is available free of charge via the Internet at http://pubs.acs.org.

■ AUTHOR INFORMATION

Corresponding Author

*E-mail: peter.hesketh@me.gatech.edu (P.J.H.); sankar.nair@chbe.gatech.edu (S.N.).

Notes

The authors declare no competing financial interest.

■ ACKNOWLEDGMENTS

This work was supported by the ConocoPhillips Company.

■ REFERENCES

(1) Kuppler, R. J.; Timmons, D. J.; Fang, Q. R.; Li, J. R.; Makal, T. A.; Young, M. D.; Yuan, D. Q.; Zhao, D.; Zhuang, W. J.; Zhou, H. C. *Coord. Chem. Rev.* **2009**, *253*, 3042−3066.
(2) Rowsell, J. L. C.; Yaghi, O. M. *Microporous Mesoporous Mater.* **2004**, *73*, 3−14.
(3) Bae, T. H.; Lee, J. S.; Qiu, W. L.; Koros, W. J.; Jones, C. W.; Nair, S. *Angew. Chem., Int. Ed.* **2010**, *49*, 9863−9866.
(4) Li, Y. S.; Liang, F. Y.; Bux, H.; Feldhoff, A.; Yang, W. S.; Caro, J. *Angew. Chem., Int. Ed.* **2010**, *49*, 548−551.
(5) Li, Y. S.; Liang, F. Y.; Bux, H. G.; Yang, W. S.; Caro, J. *J. Membr. Sci.* **2010**, *354*, 48−54.
(6) McCarthy, M. C.; Varela-Guerrero, V.; Barnett, G. V.; Jeong, H. K. *Langmuir* **2010**, *26*, 14636−14641.
(7) Achmann, S.; Hagen, G.; Kita, J.; Malkowsky, I. M.; Kiener, C.; Moos, R. *Sensors* **2009**, *9*, 1574−1589.
(8) Allendorf, M. D.; Houk, R. J. T.; Andruszkiewicz, L.; Talin, A. A.; Pikarsky, J.; Choudhury, A.; Gall, K. A.; Hesketh, P. J. *J. Am. Chem. Soc.* **2008**, *130*, 14404−14405.
(9) Biemmi, E.; Scherb, C.; Bein, T. *J. Am. Chem. Soc.* **2007**, *129*, 8054−8055.
(10) Bordiga, S.; Regli, L.; Bonino, F.; Groppo, E.; Lamberti, C.; Xiao, B.; Wheatley, P. S.; Morris, R. E.; Zecchina, A. *Phys. Chem. Chem. Phys.* **2007**, *9*, 2676−2685.
(11) Chapman, K. W.; Halder, G. J.; Chupas, P. J. *J. Am. Chem. Soc.* **2008**, *130*, 10524−10526.
(12) Venkatasubramanian, A.; Lee, J.-H.; Houk, R.; Allendorf, M.; Nair, S.; Hesketh, P. *ECS Trans.* **2010**, *33*, 229−238.
(13) Uemura, K.; Koniagawa, Y.; Yamasaki, Y.; Kita, H. *Desalination* **2008**, *234*, 1−8.
(14) Wang, Q. M.; Shen, D. M.; Bulow, M.; Lau, M. L.; Deng, S. G.; Fitch, F. R.; Lemcoff, N. O.; Semanscin, J. *Microporous Mesoporous Mater.* **2002**, *55*, 217−230.
(15) Zacher, D.; Shekhah, O.; Woll, C.; Fischer, R. A. *Chem. Soc. Rev.* **2009**, *38*, 1418−1429.
(16) Haldoupis, E.; Nair, S.; Sholl, D. S. *J. Am. Chem. Soc.* **2010**, *132*, 7528−7539.
(17) Watanabe, T.; Keskin, S.; Nair, S.; Sholl, D. S. *Phys. Chem. Chem. Phys.* **2009**, *11*, 11389−11394.
(18) Sun, P.; Jiang, Y. D.; Xie, G. Z.; Du, X. S.; Hu, J. *Sens. Actuators, B* **2009**, *141*, 104−108.
(19) Kikuchi, M.; Omori, K.; Shiratori, S. In *Proc. IEEE Sensors 2004*; Rocha, D., Sarro, P. M., Vellekoop, M. J., Eds.; IEEE: New York, 2004; Vols. *1*−*3*, pp 718−721.
(20) Quy, N. V.; Minh, V. A.; Luan, N. V.; Hung, V. N.; Hieu, N. V. *Sens. Actuators, B* **2011**, *153*, 188−193.
(21) Reyes, P. I.; Zhang, Z.; Chen, H. H.; Duan, Z. Q.; Zhong, J.; Saraf, G.; Lu, Y. C.; Taratula, O.; Galoppini, E.; Boustany, N. N. *IEEE Sens. J.* **2009**, *9*, 1302−1307.
(22) Zheng, J. B.; Li, G.; Ma, X. F.; Wang, Y. M.; Wu, G.; Cheng, Y. N. *Sens. Actuators, B* **2008**, *133*, 374−380.
(23) Huang, C. Y.; Song, M.; Gu, Z. Y.; Wang, H. F.; Yan, X. P. *Environ. Sci. Technol.* **2011**, *45*, 4490−4496.
(24) Zybaylo, O.; Shekhah, O.; Wang, H.; Tafipolsky, M.; Schmid, R.; Johannsmann, D.; Woll, C. *Phys. Chem. Chem. Phys.* **2010**, *12*, 8092−8097.
(25) Ranjan, R.; Tsapatsis, M. *Chem. Mater.* **2009**, *21*, 4920−4924.
(26) Pan, L.; Olson, D. H.; Ciemnolonski, L. R.; Heddy, R.; Li, J. *Angew. Chem., Int. Ed.* **2006**, *45*, 616−619.
(27) Lee, J.; Li, J.; Jagiello, J. *J. Solid State Chem.* **2005**, *178*, 2527−2532.
(28) Pan, L.; Sander, M. B.; Huang, X. Y.; Li, J.; Smith, M.; Bittner, E.; Bockrath, B.; Johnson, J. K. *J. Am. Chem. Soc.* **2004**, *126*, 1308−1309.
(29) Bao, Z. B.; Alnemrat, S.; Yu, L. A.; Vasiliev, I.; Ren, Q. L.; Lu, X. Y.; Deng, S. G. *J. Colloid Interface Sci.* **2011**, *357*, 504−509.
(30) Morris, W.; Doonan, C. J.; Furukawa, H.; Banerjee, R.; Yaghi, O. M. *J. Am. Chem. Soc.* **2008**, *130*, 12626−12627.
(31) Carson, C. G.; Brown, A. J.; Sholl, D. S.; Nair, S. *Cryst. Growth Des.* **2011**, *11*, 4505−4510.
(32) Park, K. H.; Koh, M. S.; Yoon, C. H.; Kim, H. W.; Kim, H. D. *J. Supercrit. Fluids* **2004**, *29*, 203−212.
(33) Lu, C. S.; Lewis, O. *J. Appl. Phys.* **1972**, *43*, 4385−4390.
(34) Johannsmann, D.; Reviakine, I.; Rojas, E.; Gallego, M. *Anal. Chem.* **2008**, *80*, 8891−8899.
(35) Janshoff, A.; Galla, H. J.; Steinem, C. *Angew. Chem., Int. Ed.* **2000**, *39*, 4004−4032.
(36) Chung, T. S.; Chan, S. S.; Wang, R.; Lu, Z. H.; He, C. B. *J. Membr. Sci.* **2003**, *211*, 91−99.
(37) Moore, T. T.; Koros, W. J. *J. Appl. Polym. Sci.* **2007**, *104*, 4053−4059.
(38) Scholes, C. A.; Tao, W. X.; Stevens, G. W.; Kentish, S. E. *J. Appl. Polym. Sci.* **2010**, *117*, 2284−2289.
(39) Poling, B. E. *The Properties of Gases and Liquids*, 5th ed.; McGraw-Hill: New York, 2001.
(40) Tomita, T.; Nakayama, K.; Sakai, H. *Microporous Mesoporous Mater.* **2004**, *68*, 71−75.
(41) Skoulidas, A. I.; Sholl, D. S. *J. Phys. Chem. A* **2003**, *107*, 10132−10141.

(42) Zheng, H.; Han, L.; Ma, H.; Zheng, Y.; Zhang, H.; Liu, D.; Liang, S. *J. Hazard. Mater.* **2008**, *158*, 577−584.